Available online at www.sciencedirect.com
ScienceDirect
International Journal of Heat and Mass Transfer 50 (2007) 412–422
International Journal of HEAT and MASS TRANSFER
www.elsevier.com/locate/ijhmt

Numerical investigation of combustion with non-gray thermal radiation and soot formation effect in a liquid rocket engine

Doyoung Byun [a,*], Seung Wook Baek [b]

[a] Department of Aerospace Engineering, Center for Advanced e-System Integration Technology, Konkuk University, 1 Hwayang-Dong, Kwangjin-Gu, Seoul 143-701, Republic of Korea
[b] Department of Aerospace Engineering, Korea Advanced Institute of Science and Technology, 373-1 Kusong-Dong, Yusung-Gu, Taejon 305-701, Republic of Korea

Received 8 June 2006; received in revised form 29 September 2006
Available online 13 November 2006

Abstract

A numerical analysis was carried out in order to investigate the combustion and heat transfer characteristics in a liquid rocket engine in terms of non-gray thermal radiation and soot formation. Governing gas and droplet phase equations with PSIC model, turbulent combustion model with liquid kerosene fuel, soot formation, and non-gray thermal radiative equations are introduced. A radiation model was implemented in a compressible flow solver in order to investigate the effects of thermal radiation. The finite-volume method (FVM) was employed to solve the radiative transfer equation, and the weighted-sum-of-gray-gases model (WSGGM) was applied to model the radiation effect by a mixture of non-gray gases and gray soot particulates. After confirming the two-phase combustion behavior with soot distribution, the effects of the O/F ratio, wall temperature, and wall emissivity on the wall heat flux were investigated. It was found that the effects of soot formation and radiation are significant; as the O/F ratio increases, the wall temperature decreases. In addition, as the wall emissivity increases, the radiative heat flux on the wall increases.

Keywords: Liquid rocket engine; Spray combustion; Soot formation; Non-gray radiation; Finite-volume method (FVM); Weighted-sum-of-gray-gases model (WSGGM)

1. Introduction

Numerical modeling of spray two-phase turbulent reacting flows has significant application related to the development of various power generating devices; among them furnaces, internal engines, gas turbines and liquid rocket engines. In the last two decades, the related computational performance has been greatly increased, and computational methods for spray combustion have been developed considerably to the point that accurate predictions of the hydrodynamics and thermal characteristics of dispersed spray droplets and turbulent flames are common [1–3]. However, combustion chambers involving liquid fuel propulsion systems represent very complicated phenomena in this area. The complexity originates from the existence of multiple phases and processes with very different time and length scales within the same physical domain. Accurate predictions of engine performance require detailed modeling of fluid flow, heat transfer, and combustion processes. In these flows, two-way coupling in terms of momentum, heat and mass exchange between gas and dispersed liquid droplets play an important role in fuel and oxidizer mixing and combustion [4].

To predict the characteristics of gas and droplets dynamics, an Eulerian formulation is applied for the continuous phase and a Lagrangian formulation is applied to track the motion and thermodynamic behavior of the discrete phase. The Lagrangian approach treats the droplets

* Corresponding author. Tel.: +82 2 450 4195; fax: +82 2 444 6614.
E-mail address: dybyun@konkuk.ac.kr (D. Byun).

0017-9310/$ - see front matter © 2006 Elsevier Ltd. All rights reserved.
doi:10.1016/j.ijheatmasstransfer.2006.09.020

as discrete entities in a turbulent flow field, and their trajectories are calculated. This approach has the flexibility of being able to process a poly-dispersed spray and with it the two-way coupling is typically accomplished through the particle-source-in-cell (PSIC) technique [5].

The computational methods for solving Navier–Stokes equations are largely classified into either density-based or pressure-based methods. These two methodological approaches have individual advantages and disadvantages. The basic merit of the density-based method is in its accuracy and robustness, especially with a high speed flow simulation. However, this algorithm is often ineffective with low Mach number flows due to the stiff eigenvalues of such systems. The density-based method completely breaks down at the incompressible limit, where the density is independent of the pressure and the pressure term in the momentum equation becomes singular. In the pressure-based method, the pressure–density–velocity coupling is handled by a Poisson-type pressure or a pressure correction equation derived from the continuity equation, momentum equation, and equation of state. This algorithm is relatively easy to apply to flows of all speeds [6–8]. As the pressure-based method normally employs a sequential solution procedure, it requires less computer memory and computing time. Several research efforts have sought to develop pressure-based methods for flow calculations for all speeds [6–8]. In this study, a pressure-based algorithm is used to solve the Navier–Stokes equation, and the finite-volume method is adopted to discretize all of the equations.

Thus far, in terms of soot formation, the effects of thermal radiation have not been clearly investigated in liquid rocket engines. A small number of researchers have investigated the radiative heat transfer, and found that radiative effects on the wall heat transfer may be significant in scramjet combustors and chemically reacting nozzles [9,10]. Badinand and Fransson [11] stressed the importance of thermal radiation in film-cooled LH/LOX rocket engines. They found that while radiative heat transfer may play a minor role in comparison to convection, it should not be neglected when an exact description of the heat loads to the wall for an engine is required. Because both the efficiency and the price per kilogram in orbit are of great importance as the size of an engine increases, the radiative heat transfer effect should be precisely analyzed.

More recently, the calculation of radiative transfer within a sooty turbulent ethylene-air diffusion jet flame was carried out using a Monte Carlo method and an accurate CK model for the gases [12]. Soot particles play a highly important role in the global radiative heat loss, but the influence of gaseous species such as CO_2 or H_2O are also important in the local energy balance. Until now, there has been little in-depth study on the effect of the radiative heat transfer with soot formation in the liquid rocket engine.

In the present study, a pressure-based algorithm based on the Eulerian–Lagrangian formulation was developed in order to simulate the spray combustion at all speeds in the rocket engine. The PSIC model is adopted to trace the droplet motions and to calculate the characteristics of the vaporizing droplets. However, other effects of dense sprays, such as droplet collisions, break-ups, and coalescences are not included. A non-gray finite-volume radiation model is applied in order to investigate the radiation effect in turbulent combustion conditions. Additionally, the soot formation and the effect of radiation on the flow field and heat transfer are investigated.

2. Governing equation

2.1. Governing equations for gas phase

The two dimensional, unsteady, compressible, density-weighted time-averaged Navier–Stokes equations and conservation equations for the mass, energy, turbulent kinetic energy, and the eddy dissipation rate of the two-equation model as well as for species for a chemically reacting flow is written as follows in a general form [4]:

$$\frac{\partial(\rho\phi)}{\partial t} + \mathrm{div}(\rho\vec{U}\phi) - \mathrm{div}(\Gamma_\phi \mathrm{grad}\phi) = S_{\phi,\mathrm{g}} + S_{\phi,\mathrm{l}} \tag{1}$$

where ϕ is any one of the dependent variables, $\vec{U}$ is the gas velocity vector, ρ is the gas density and Γ represents the exchange coefficient such as the diffusion coefficient. $S_{\phi,\mathrm{g}}$ and $S_{\phi,\mathrm{l}}$ are the source terms that stem from the turbulent gas field and the interaction between the droplet and the gas, respectively. These are represented in Table 1. In Table 1, the exchange coefficients and source terms for each conservation equation are presented. The effective viscosity, μ_{eff}, contains both molecular and turbulent eddy viscosities, i.e., $\mu_{\mathrm{eff}} = \mu + \mu_{\mathrm{T}}$. The energy equation contains two different source terms due to chemical reaction and radiation. Here, $\dot{\omega}_{\mathrm{f}} Q_{\mathrm{f}}$ is the source term due to combustion, while $-\nabla \cdot q^{\mathrm{R}}$ represents the radiation source term.

All of the transport properties used in this study have been derived from the database of physical property information developed by Daubert and Danner [13]. Once the individual species viscosities and conductivities are found, the mixture viscosity and conductivity are computed using Wilke's mixing rule [14].

2.2. Governing equations for liquid phase

The liquid phase is traced by solving Lagrangian equations of motion and transport for the life histories of a statistically significant sample of individual droplets. The spray model used in this study is based on a dilute spray assumption which is valid in regions where the droplet loading is low. The liquid fuel and liquid oxygen is assumed to enter the combustor as a fully atomized spray comprised of spherical droplets. The present model does not account for the effects due to droplet breakup and coalescence processes, which might be significant in a dense spray situation, and due to interaction between droplet and

Table 1
Variables and source terms of the governing equations for the gas phase

Equation	ϕ	Γ_ϕ	$S_{\phi,g}$	$dV_\phi S_{\phi,l}$
Continuity	1	0	0	$\sum n_p \dot{m}_p$
Momentum	u_i	0	$-\frac{\partial p}{\partial x_i}+\frac{\partial}{\partial x_j}(\tau_{ij})-\frac{2}{3}\frac{\partial \rho k}{\partial x_i}$	$\sum\left(n_p \dot{m}_p u_{p,i}-\frac{\rho\pi d_p^3 n_p}{6}\frac{du_{p,i}}{dt}\right)$
Energy	h	$\frac{\mu}{Pr}+\frac{\mu_t}{\sigma_h}$	$\frac{DP}{Dt}+\Phi-\dot{w}_f Q_f-\nabla\cdot q^R$	$\sum\{n_p \dot{m}_p h_{fv}-\dot{q}_{gp}\}$
k-equation	k	$\frac{\mu_{eff}}{\sigma_k}$	$G_k-\rho\varepsilon$	0
ε-equation	ε	$\frac{\mu_{eff}}{\sigma_\varepsilon}$	$c_1\frac{\varepsilon}{k}G_k-c_2\rho\frac{\varepsilon^2}{k}$	0
Species	Y_i	$\frac{\mu_{eff}}{Sc_t}$	$\dot{\omega}_i$	If i = fuel, LOX $\sum n_p \dot{m}_p$ Others 0

$$\mu_{eff}=\mu+\mu_t$$

$$\tau_{ij}=2\mu_{eff}\varepsilon_{ij}+\beta\varepsilon_{kk}\delta_{ij},\quad \varepsilon_{ij}=\frac{1}{2}\left(\frac{\partial u_i}{\partial u_j}+\frac{\partial u_j}{\partial x_i}\right)$$

$$\beta=-\frac{2}{3}\mu_{eff},\quad \delta_{ij}=\text{Kronecker delta function}$$

$$\Phi=\tau_{ij}\frac{\partial u_i}{\partial x_j},\quad \frac{Dp}{Dt}=\frac{\partial p}{\partial t}+u_j\frac{\partial p}{\partial x_j}$$

$$h=\sum_k Y_k\int_{T_{ref}}^{T} C_{p,k}dT$$

$$G_k=\mu_{eff}\frac{\partial u_i}{\partial x_j}\left[\frac{\partial u_i}{\partial x_j}+\frac{\partial u_j}{\partial x_i}\right]$$

$$C_\mu=0.09,\quad C_1=1.44,\quad C_2=1.92,\quad \sigma_k=0.9,\quad \sigma_\varepsilon=1.3,\quad \sigma_h=0.9,\quad Sc_i=0.9$$

turbulence. The Lagrangian equations [4] governing the droplet motion are

$$m_p\left(\frac{du_{p,i}}{dt}\right)=\frac{1}{2}\rho C_D(u_i-u_{p,i})\left|\vec{u}-\vec{u}_p\right|A_p-\left(\frac{m_p}{\rho_p}\frac{\partial p}{\partial x_i}\right) \tag{2}$$

$$\frac{dx_i}{dt}=u_{p,i} \tag{3}$$

where m_p is the mass of the droplet and $\vec{u}_p$ its velocity vector. C_D is the drag coefficient and ρ, $\vec{u}$, and p are the density, velocity vector, and pressure of the gas phase, respectively. A_p is the droplet surface area, πd_p^2, and m_p/ρ_p denotes the droplet volume, $\pi d_p^3/6$. The first term on the right side of Eq. (2) accounts for effects of drag with gas and the second term for the local pressure gradient. However, the present model does not take into account the effects of droplet break-up, coalescence processes, and a body force such as gravity. The equation above can be integrated using the second order Runge–Kutta method so that the droplet velocity can be obtained and the droplet position can be traced. The drag coefficient, C_D, for the droplet is based on the local Reynolds number evaluated as,

$$Re_p=\frac{\rho d_p|\vec{u}-\vec{u}_p|}{\mu} \tag{4}$$

The following correlation has been found to be valid for different ranges of the Reynolds number [15]:

$$C_d = 24(1 + 0.15Re^{0.687})/Re_p \quad \text{for } Re_p < 10^3$$
$$C_d = 0.44 \quad \text{for } Re_p > 10^3 \tag{5}$$

The mass conservation equation for the droplet is given by,

$$\frac{dm_p}{dt} = \dot{m}_p = 2\pi d_p \rho D \ln(1+B) Nu \tag{6}$$

where d_p is diameter of the droplet, D is the diffusion coefficient, B denotes Spalding's number, and Nu is the Nusselt number. Following the Ranz–Marxhall's experimental correlation [15], the Nusselt number is,

$$Nu = 2 + 0.6Re_p^{1/2}Pr^{1/3} \tag{7}$$

where Pr is the Prantl number. The Spalding number, B, is defined as,

$$B = \frac{Y_{fs} - Y_f}{1 - Y_{fs}} \tag{8}$$

where Y_{fs} and Y_f are the fuel vapor mass fraction at the surface of the droplet and the mean fuel mass fraction of the ambient gas, respectively. Y_{fs} is obtained from the following equation

$$Y_{fs} = \frac{X_{fs}W_f}{X_{fs}W_f + (1 - X_{fs})W_{oxi}} \tag{9}$$

where X_{fs} is the mole fraction of fuel vapor at the droplet surface, W_f is the molecular weight of fuel, and W_{oxi} is the molecular weight of gas mixture excluding the fuel vapor. Based on the assumption of Raoult's law [14], the mole fraction, X_{fs}, at the droplet surface is equal to the ratio of the partial pressure of fuel vapor to the total pressure, p_{vap}/p. Here, p_{vap} is the partial vapor pressure [13]. The energy equation for the droplet is written as,

$$m_p C_{p,p} \frac{dT_p}{dt} = Nu\pi k d_p(\widetilde{T}_g - T_p) - L\dot{m}_p \tag{10}$$

where L is the latent heat of vaporization, $C_{p,p}$ is the specific heat of the liquid droplet, and k is the thermal conductivity of the gas phase. In addition, T_p is the droplet surface temperature and $\widetilde{T}_g$ is the mean gas temperature evaluated as follows:

$$\widetilde{T}_g = \frac{2}{3}T_g + \frac{1}{3}T_p \tag{11}$$

The variation of the diameter of the droplet due to vaporization is obtained as

$$-\frac{d}{dt}\left(\frac{\rho_p \pi d_p^3}{6}\right) = \dot{m}_p \tag{12}$$

where $\dot{m}_p$ is calculated by Eq. (6).

2.3. The global combustion chemistry

The spray combustion model used in this study is based on the assumption that liquid droplets act as distributed sources of fuel vapor. The implication of the combustion model is that the chemical reaction is treated in a similar way to that used for turbulent diffusion flames. The combustion of kerosene with air in an idealized irreversible infinitely fast one-step reaction is considered and, consequently, the eddy dissipation concept is used. Actually, multi-step chemical kinetics for Kerosene and pure oxygen is necessary to describe the detailed chemical reactions. However, because here the main objective is to investigate the effect of radiative heat transfer in the engine typically due to the existence of non-gray gases as well as soot particles, we simply model the chemical reaction to get the overall thermal conditions. The reaction in the idealized irreversible single step is considered as,

$$C_nH_m + \nu_{O_2}O_2 + \nu_{N_2}N_2 \rightarrow \nu_{CO_2}CO_2 + \nu_{H_2O}H_2O + \nu_{N_2}N_2 \tag{13}$$

When the combustion processes are kinetically controlled, the fuel dissipation rate is controlled by the Arrhenius rate expression:

$$\dot{\omega}_f = A[C_{fuel}]^a[C_{O_2}]^b \exp\left[-\frac{E_a}{R'T}\right] \tag{14}$$

where A is the Arrhenius factor (2.8×10^{15}) and E_a is activation energy(45). a and b are 1 and 0.8, respectively [2]. The major components of the kerosene are alkanes (79% by weight), with the other components being aromatics (11%), and cyclanes (10%). Among the alkanes, C_{10} to C_{13} compounds are predominant, while the main components of the aromatic hydrocarbons and the cyclanes are C_9 to C_{10} hydrocarbons. The general formula is $C_{11}H_{22}$ [2].

The influence of turbulent intermittence on the finite rate chemistry is modeled using a simple eddy dissipation concept. This mixing-controlled rate of reaction is related to local properties such as density, turbulent time scale k/ε, and the chemical species mass fraction. The reaction rate of the fuel is taken as the smallest or the slowest of the turbulent dissipation rates of fuel and oxygen. The eddy dissipation model for the turbulent combustion flow can express the chemical reaction rate as [16],

$$\dot{\omega}_f = -C_R \rho \frac{\varepsilon}{k} \min\left[Y_{fuel}, \frac{Y_{O_2}}{s}\right] \tag{15}$$

where s is the stoichiometric oxygen/fuel ratio and the constant of C_R is 4.0.

Finally the reaction rate is taken as the slowest value from the results of Eqs. (14) and (15).

2.4. The soot formation and oxidation model

As the radiative properties of combustion products depend significantly upon the sootiness of the flame, a model for soot formation and oxidation is necessary to

appropriate a model of the radiation. Soot formation and oxidation were modeled using a two-step global scheme, and the model parameters were presented for several hydrocarbon fuels [17]. The soot model is based upon a solution of balance equations for soot number density, n, and the soot volume fraction, f_v. To facilitate the representation of these quantities in Favre-averaged balance equations, the soot number density, n, and soot volume fraction, f_v, are replaced by $\phi_n = \frac{n}{\rho N_o}$ and $\phi_f = \frac{\rho_s}{\rho} f_v$, respectively. N_o denotes Avogadro's number (6×10^{26}) and ρ_s represents the soot density (assumed to be 1800 kg/m^3). The balance equations with source terms are as follows:

$$\mathrm{div}(\rho \vec{U} \phi_n) - \mathrm{div}\left(\frac{\mu_{\mathrm{eff}}}{\sigma_{\phi_n}} \mathrm{grad}\phi_n\right) = \frac{\mathrm{d}\phi_n}{\mathrm{d}t} \tag{16}$$

$$\mathrm{div}(\rho \vec{U} \phi_f) - \mathrm{div}\left(\frac{\mu_{\mathrm{eff}}}{\sigma_{\phi_f}} \mathrm{grad}\phi_f\right) = \frac{\mathrm{d}\phi_f}{\mathrm{d}t} - \dot{\omega}_{s,ox} \tag{17}$$

The reduced mechanism distinguishes the processes of nucleation, surface growth and coagulation in the rate of expressions of the form

$$\frac{\mathrm{d}\phi_n}{\mathrm{d}t} = \alpha - \rho^2 \beta \phi_n^2 \tag{18}$$

$$\frac{\mathrm{d}\rho_s f_v}{\mathrm{d}t} = v f_v^{2/3} n^{1/3} + \delta \tag{19}$$

where

$$\begin{aligned} \alpha &= C_\alpha \rho^2 T^{1/2} X_{\mathrm{fuel}}^{M_\alpha} \exp(-T_\alpha/T) \\ \beta &= C_\beta T^{1/2} \\ v &= C_v \rho T^{1/2} X_{\mathrm{fuel}}^{M_v} \exp(-T_v/T) \\ \delta &= 144\alpha \end{aligned} \tag{20}$$

Here, α and δ represent the influence of nucleation on the number density and the soot volume fraction, respectively, while β and v characterize the processes of coagulation and surface growth, respectively. Comparing the predicted distributions of soot volume fraction with the measured distribution, Stewart et al. [17] present the following set of model parameters for non-premixed kerosene-air flames:

$$\begin{aligned} &C_\alpha = 5.3 \times 10^6 [\mathrm{m^3\ K^{-1/2}\ kg^{-2}\ s^{-1}}] \\ &C_\beta = 1.2 \times 10^{15} [\mathrm{m^3\ K^{-1/2}\ s^{-1}}] \\ &C_v = 7.8 \times 10^6 [\mathrm{m\ K^{-1/2}\ s^{-1}}] \\ &M_\alpha = 2, \quad M_v = 5 \\ &T_\alpha = 21{,}000, \quad T_v = 12{,}600\ [\mathrm{K}] \end{aligned} \tag{21}$$

The soot oxidation rate is described by the model which assumes, by an analogy to gas turbulent combustion, that the process is mixing-controlled and that the reaction rate is limited by the locally lean concentration [18],

$$\dot{\omega}_{s,ox} = \rho A \frac{\varepsilon}{k} \min\left[\phi_f, \frac{Y_0}{v_s} \frac{\phi_f v_s}{\phi_f v_s + Y_{fu} v_0}\right] \tag{22}$$

where v_s is the mass stoichiometric coefficient of the oxidizer in the soot oxidation reaction.

2.5. Radiative transfer equation

When a quantity of emitting and scattering particles or non-scattering soot particulates are suspended in a radiative gas medium, the radiative transfer equation (RTE) governing the spectral change of radiative intensity can be written as [19]:

$$\begin{aligned} \frac{\mathrm{d}I_\eta}{\mathrm{d}s} &= -(\kappa_{g,\eta} + \kappa_{s,\eta} + \sigma_{s,\eta}) I_\eta + \kappa_{g,\eta} I_{g,b\eta} + \kappa_{s,\eta} I_{s,b\eta} \\ &\quad + \frac{\sigma_{s,\eta}}{4\pi} \int_{4\pi} \Phi_\eta(\hat{s}, \hat{s}') I_\eta(\hat{s}') \mathrm{d}\Omega' \end{aligned} \tag{23}$$

where $\kappa_{g,\eta}$ and $\kappa_{s,\eta}$ are the absorption coefficients of gas and soot at the specific wave number η, respectively. In addition, $\sigma_{s,\eta}$ is the scattering coefficient, and $\Phi(\hat{s}, \hat{s}')$ is the scattering phase function for radiation from incoming direction $\hat{s}'$ to scattered direction $\hat{s}$.

This study assumes a mixture of non-gray gases and gray soot particulates. Although the particle absorption coefficients depend on such factors as the incident electromagnetic wave, incident direction, or the emission direction, Skocypec et al. [20] experimentally showed that the emittance due to particulate can be considered gray, thus the postulation above may be acceptable here.

Due to the existence of the soot particles, the absorption coefficient may be increased in almost combustion chambers and the effect of the radiative heat transfer may play a more important role in the heat transfer modes. Yu et al. [19] presented weighting factors used in the WSGGM for a mixture of non-gray gas and gray particles. Similarly, in this study, the WSGGM is applied to factor in the non-gray effect of CO_2 and H_2O gases with gray soot particles. According to Modest [21] and Adams and Smith [22], the soot absorption coefficient is defined as

$$\kappa_s = \frac{3.72 f_v C_0 T}{C_2} \tag{24}$$

where $C_2 = 1.4388$ cm K, and $C_0 = 5.5$ are used.

3. Numerical methods

To solve the above Navier–Stokes equations in a body-fitted coordinate system, the SIMPLE algorithm [6–8] was adopted. Its major characteristics are (1), the use of a collocated (non-staggered) grid system; and (2), the use of Cartesian velocity components as dependent variables. A non-staggered scheme facilitates efficient computer programming, as all of the variables are considered in the same control volume. In particular this advantage is viable for the treatment of the source term and interface condition in the two-phase flow. The computational methods for solving Navier–Stokes equations are largely classified as density-based and pressure-based methods. These two methodological approaches have individual merits and disadvantages. The basic merit of the density-based method is its accuracy and robustness, especially high speed flow simulation. However, this algorithm is often ineffective at low Mach number

flows due to the stiff eigenvalues of the system. The density-based method completely breaks down at the incompressible limit, where the density is independent of the pressure and the pressure term in the momentum equation becomes singular. In the pressure-based method, the pressure–density–velocity coupling is handled by the Poisson-type pressure or pressure correction equation derived from the continuity, momentum equations, and equation of state. This algorithm is relatively easy to apply to flows at all speeds [6–8].

There are several research efforts to develop pressure-based methods for the flow calculations at all speeds [7,8]. Here the pressure-based algorithm is used to solve the Navier–Stokes equation and the finite volume method is adopted to discretize all of the governing equations. In the incompressible flows, following the SIMPLE algorithm [6], once the pressure correction equation has been solved for, the velocities and pressure are updated

$$u^m = u^{m-1} + u', \quad p^m = p^{m-1} + p' \tag{25}$$

where m means iterations. From these equations, the relation between the velocity and pressure corrections is obtained. Then application of the discretized continuity equation to this velocity correction leads to pressure correction equation. On the other hand, in compressible flows, the mass flux depends on both the velocity component as well as the density. To correct the mass flux imbalance, both the velocity and density should be corrected. The correctness of the mass flux on the face "e" of a control volume can be expressed as

$$\dot{m}_e^m = (\rho^{m-1} + \rho')_e (u_n^{m-1} + u_n')_e S_e \tag{26}$$

where ρ', u_n', and S_e represent the density and normal velocity corrections, and control surface area at "e" face, respectively. The mass flux correction is thus

$$\dot{m}_e' = (\rho^{m-1} S u_n')_e + (u_n^{m-1} S \rho')_e + \underline{(u_n' S \rho')_e} \tag{27}$$

The underscored term is neglected as it is of the second order in the corrections. The first term in the remaining mass flux correction is identical to the one obtained for incompressible flow. The second term is due to compressibility and represents the correction to density, which can extend the SIMPLE method to compressible flows. If the temperature is regarded as fixed for one iteration, the density correction can be written as

$$\rho' \approx \left(\frac{\partial \rho}{\partial p}\right)_T p' = C_\rho p' \tag{28}$$

where the coefficient C_ρ can be determined from the equation of state for a perfect gas, $C_\rho = \left(\frac{\partial \rho}{\partial p}\right)_T = \frac{1}{RT}$. Finally, the mass flux corrections such as Eq. (27) are substituted into the continuity equation, an algebraic system of pressure correction equation can be derived [6–8].

Based on the mathematical modeling and numerical analysis described, a computer codes have been developed to simulate two-dimensional turbulent chemically reacting flows at all speeds. To validate the computer codes, the present collocated finite-volume method for predicting the compressible flows has been applied to analyze the flow for a converging–diverging planar nozzle reported by Karki and Patankar [8]. The planar nozzle geometry is given in Fig. 1(a). The calculation has been performed by using a $(N_x \times N_y) = (100 \times 50)$ grid system for the half nozzle. The no-slip condition was used at the wall and the inlet mach number was taken as 0.232 and the ratio of the exit static pressure to the upstream stagnation pressure was fixed at 0.1135, corresponding to the experimental condition. In Fig. 1(b), the pressure distribution at the wall and the center line are compared with the experimental results. The current numerical results are in very good agreement with the experimental results.

The separated computations for the gas and liquid phase flow fields and the iterative exchange of interfacial transfer data entails an artificial decoupling of both phases. In particular, for two-phase flows with intense-phase interaction, this effect leads to a critical overestimation of droplet source terms in the first iteration. To predict the characteristics of liquid fuel and oxygen droplets dynamics, a Lagrangian formulation is applied to track the motion and thermodynamic behavior of the discrete phase. The Lagrangian approach treats the droplets as discrete entities in a turbulent flow field, and their trajectories are

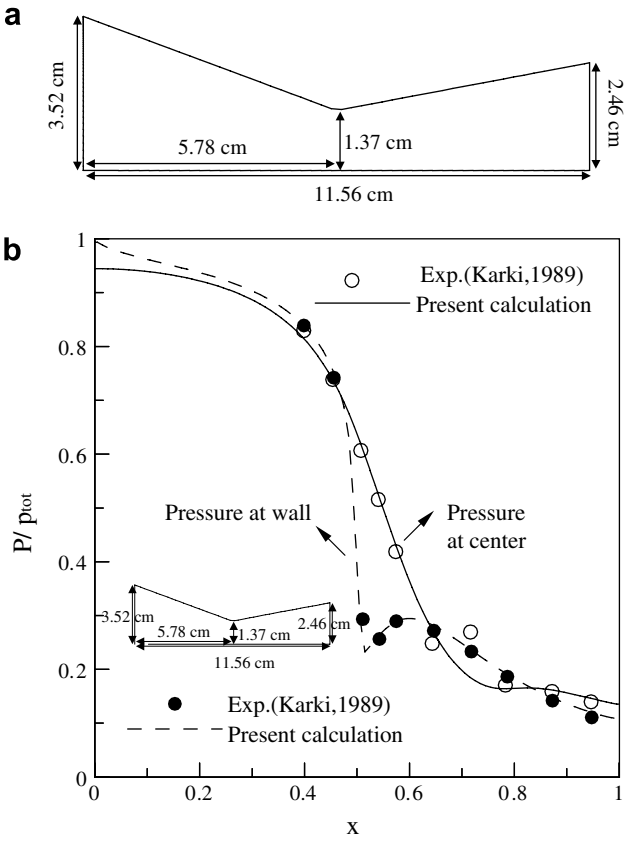

Fig. 1. Incompressible and compressible flow in converging and diverging nozzle: (a) schematic of planar converging–diverging nozzle, (b) comparisons of pressure distributions at the centerline and the upper wall.

calculated. This approach has the flexibility of being able to process a poly-dispersed spray and with it the two-way coupling is typically accomplished through the particle-source-in-cell (PSIC) technique [5]. Droplet motion and energy equations are integrated using second order Runge–Kutta method.

At a wall, no-slip conditions, zero normal stress and an adiabatic condition are applied. At the inlet, the total temperature, total pressure, and the traverse velocity components are specified [6]. At the outlet boundary, the information for flow is rarely known. To determine approximations at the boundary, an extrapolation along grid lines from the interior to the boundary is normally utilized. At a symmetry plane, the convective fluxes of all quantities are zero. Additionally, the normal gradients of the velocity parallel to symmetry plane and of all the scalar quantities there are zero.

A derivation of the finite-volume method for radiation has already been described and is common in the literature, thus it is recommended to refer to them for more details [23,24]. The flux methods such as finite volume method (FVM) used to show a non-physical oscillation in a solution on the boundary heat flux, which results from the ray effect. This wiggling behavior is caused by the finite discretization of the continuous control angle. Byun et al. [23] presented that the ray effect is found to be more conspicuous when the heat source is locally isolated in the rather cold medium. However, if the temperature distributions in the domain are almost uniform such as rocket engine, the ray effects is not significant so that the FVM can be applied to analyze the radiative heat transfer.

4. Results and discussion

Fig. 2 shows an axisymmetric schematic diagram of a typical liquid fuel rocket and spatial grid system. The length of the rocket is 0.89 m and the cross sectional areas of the throat and the exit are 0.075 and 0.38 m^2. The spatial grid system used in this figure is $(N_x \times N_y) = (80 \times 60)$. In this study, an impinging-type injector is considered; this is composed of two fuel jets and two additional oxygen jets between the fuel jets on the same plane. This type of injector is commonly used in liquid propellant rockets where fuel is injected from the side jets and an oxidizer from the central parallel jets. For this type of injector, there is little research that investigates the fragmentation and atomization of fuel and oxidizer droplets. Therefore, the spray droplets are assumed to be injected from a source point where the impinging jets collide with each other. The initial droplet velocity magnitude is set as 32.5 m/s and 27.0 m/s for the fuel and oxidizer respectively. From the experimental results, the diameter of the kerosene droplet is considered to be 68 μm and that of the liquid oxygen 54 μm [25]. This atomization model inherently assumes that the spray is dilute; however, this is not necessarily valid near an injector.

Liquid fuel and oxygen are injected into the rocket combustor at a temperature of 300 K and 90 K, respectively. The pressure inside the chamber is 20 atmospheric pressures. The liquid fuel mass flow rate is 8.1 kg/s, and the liquid oxygen mass flow rate is determined from the mixing ratio. The control angle system used here is $(N_\theta \times N_\phi) = (12 \times 8)$ for the radiation calculation. All of the outside walls are assumed to be isothermal and gray in order to investigate the effect of the radiation. The inlet and outlet surfaces are treated as pseudo-black walls. For the radiative transfer equation, the temperature of the inlet surface is equal to the liquid fuel temperature, and that of the outlet surface is determined as an infinite temperature.

The specific objective of this study is to simulate the spray combustion in the liquid fuel rocket engine and to investigate the soot formation and the radiative heat transfer to the nozzle wall. The problem considered in this study contains three parameters: (1) the overall mixture ratio of oxygen to kerosene; (2), the wall temperature; and (3), the wall emissivity. A numerical simulation was performed for a variety of combinations of these parameters. For gas radiation, the important radiating species are H_2O and CO_2. As the concentration of OH is approximately 10–20 times less than that of H_2O, the contribution of radiation from OH is neglected [9].

Fig. 3 illustrates the contours of the reaction rate, isotherm, isobaric, and the H_2O and CO_2 mass fractions. The vaporized fuel and oxygen move downward along with the main convective currents and are mixed with each other near the injector. As soon as the mixing occurs, the reaction takes place, as shown in Fig. 3(a). Therefore, a significant amount of reaction is observed near the injector and the reaction is mainly related to the mixing-controlled mechanism. It is clear that the maximum reaction rate is

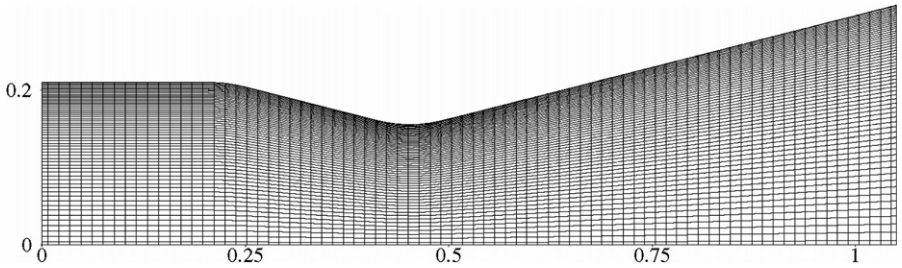

Fig. 2. Schematic of the liquid fuel rocket combustor and grid system.

formed in the region where the fuel and oxygen are actively mixed and where the turbulent quantities are more active, and where a high temperature is found in the central zone. As an exothermic chemical reaction takes place readily, the temperature increases together with the flow and has a maximum at the inner core region of the combustion chamber before the nozzle throat. When the flow passes through the nozzle, supersonic expansion plays a major role such that the temperature and pressure decrease. Although the chemical reaction simultaneously occurs in the nozzle, it becomes very weak due to the large consumption of fuel and oxygen in the combustion core region.

In addition to the non-gray gas radiation, the radiative effect by luminous soot particulates is also considered. Fig. 4 describes the contour of the $\phi_f = \frac{\rho_s}{\rho} f_v$ and volume fraction in a liquid rocket engine. The soot volume fraction necessary for a calculation of the absorption coefficient is obtained from the values of ϕ_f. As the density variation is very large along the downstream, the volume fraction shows peak in the combustion core region. For this reason, the formation of soot mainly affects the radiative heat transfer in the combustion chamber rather than in the nozzle, while the most of the H_2O and CO_2 species reside in the nozzle and chiefly affect the thermal field in the nozzle. The

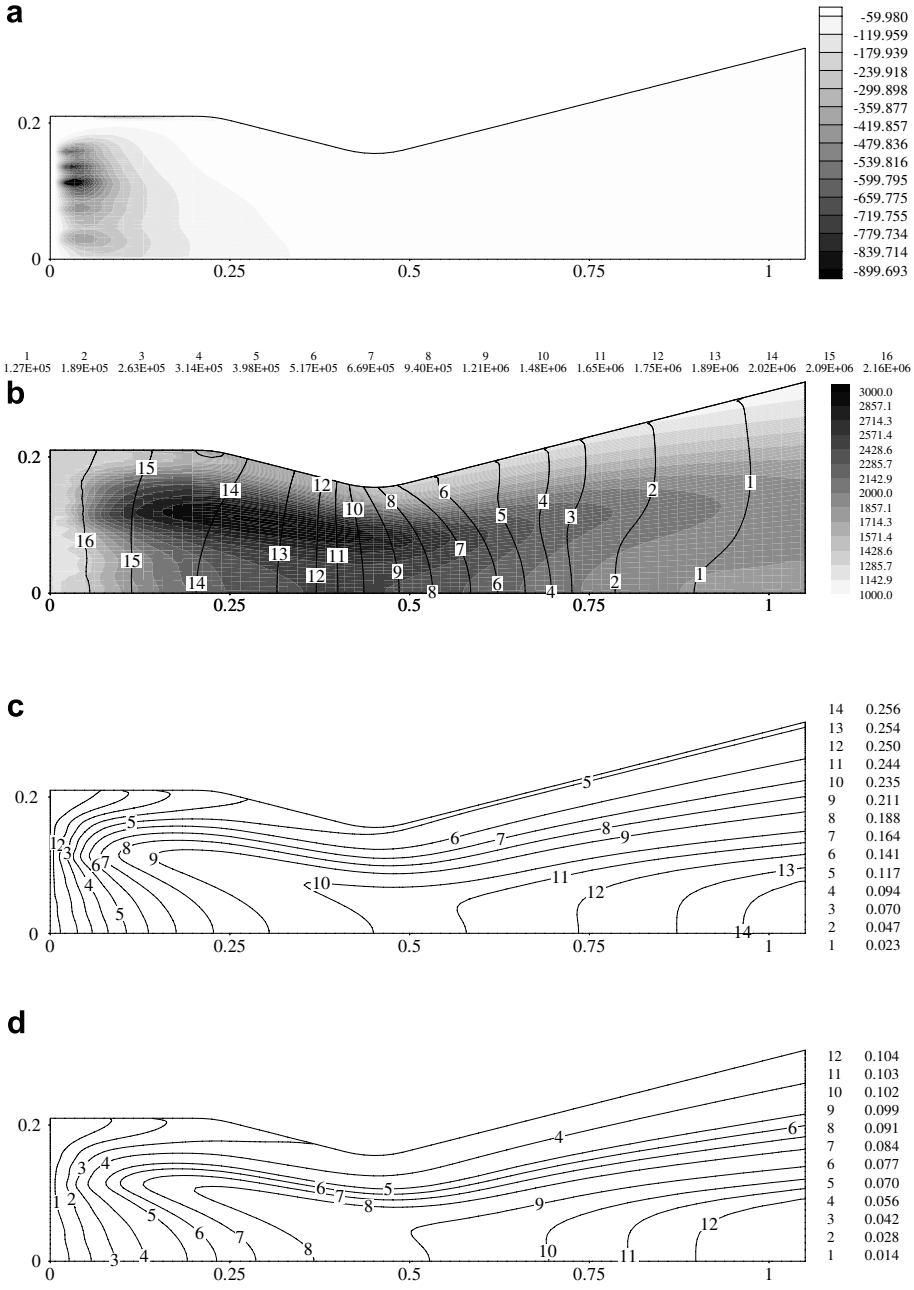

Fig. 3. Contours of reaction rate, temperature, pressure, and H_2O and CO_2 mass fractions: (a) reaction rate, (b) temperature and pressure, (c) H_2O mass fraction, (d) CO_2 mass fraction.

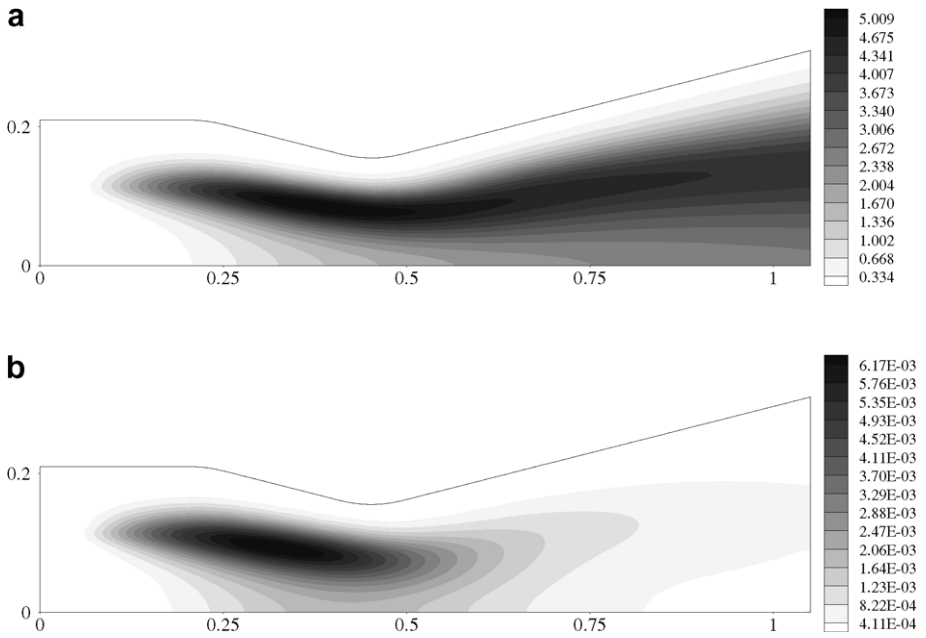

Fig. 4. Contour of soot mass fraction and volume fraction. (a) ϕ_f, (b) soot volume fraction.

soot volume fraction reaches a peak of 10^{-3} order of magnitude. The influence of pressure on soot formation has been extensively investigated in premixed and non-premixed flames [26,27]. The measurements suggest pressure dependence for the soot volume fraction, of a general form:

$$f_v \propto p^n \quad (1 \leqslant n \leqslant 2) \tag{25}$$

Young et al. [26] observed the substantially linear growth of the soot formation rate with pressure. At a high pressure, the peak soot volume fractions are located on the flame centerline, and the centerline soot volume fraction can reach a value of 10^{-4} at 10 bar. Due to the large amount of soot formation, the radiation effect on thermo-fluid dynamic structure increases.

Fig. 5 illustrates the conductive heat flux to the wall with and without radiation. The conductive heat flux on the wall is defined as $q_{cwall} = -k(T_{wall})(\partial T/\partial n)_{wall}$, where n represents direction normal to the wall [9]. An estimate of the convective heat transfer rate on the wall is a difficult task, especially for a supersonic flow such as that of a nozzle. Therefore, although the upper definition is only an approximation using the temperature difference between the wall and gas field, the conductive heat transfer is used in this study. When the radiation is included, the temperature near the wall increases and the conductive heat flux is then larger than in the case without radiation, as seen in Fig. 5.

Fig. 6 demonstrates the importance of the radiative heat transfer on the wall by the soot, showing a comparison of the radiative and conductive heat fluxes. When the soot formation is included, the radiative heat flux is larger than the conductive heat flux. On the other hand, without considering the soot formation, the radiative heat flux by only non-gray gases is smaller than the conductive heat flux,

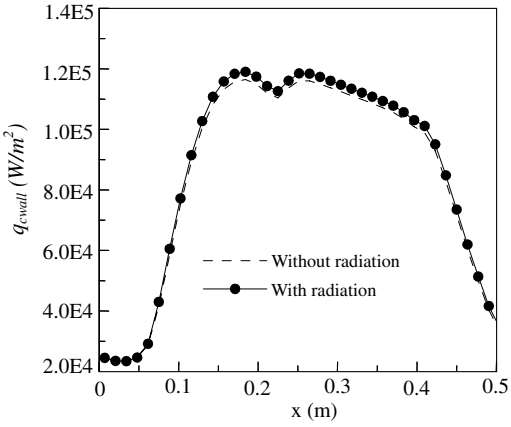

Fig. 5. Comparison of conductive heat flux on the wall with/without radiation.

while the effect of the gas radiation is not negligible. The radiative heat flux increases to the nozzle throat and then begins to decrease due to the supersonic expansion. Near the injector plane, the radiative heat flux is observed to rapidly decrease due to the pseudo-black cold injector surface.

The effects of the overall mixture ratio of oxygen to fuel on the wall heat fluxes are illustrated in Fig. 7. In this case, the overall mixture ratio of oxygen to kerosene varies from 2.0 to 2.5 and the wall temperature and the wall emissivity are 1100 K and 1.0, respectively. As the mixture ratio increases from 2.0 to 2.5, the peak flow temperature near the chamber center region increases from 2530 K to 3306 K. Because the temperature increases, the radiative heat flux increases from the hot gas to the wall. Near the wall, variations of the temperature are relatively slight, thus the change of the conductive heat flux is minuscule.

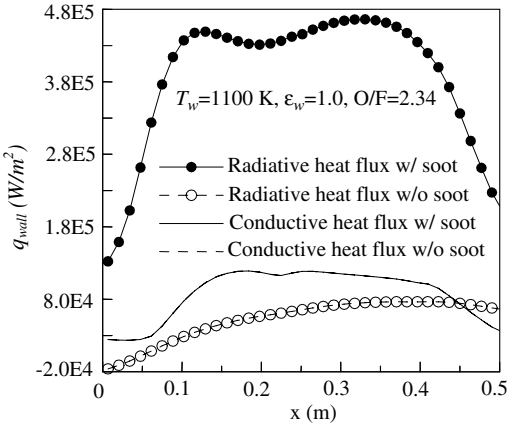

Fig. 6. Comparison of conductive and radiative heat fluxes on the wall.

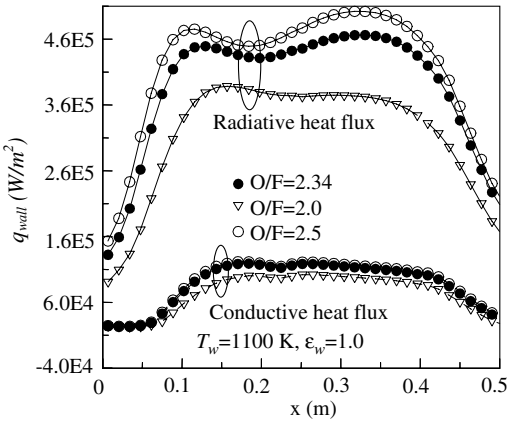

Fig. 7. Comparison of conductive and radiative heat fluxes on the wall for O/F ratios.

Fig. 8 shows the effects of the wall temperature on the heat fluxes. The overall mixture ratio of oxygen to kerosene and the wall emissivity are 2.34 and 1.0, respectively. The change in the wall temperature was found to have little influence on the combustion characteristics. Consequently, the flow temperature, pressure, H_2O mass fraction, and soot volume fraction remain nearly constant as the wall temperature varies from 800 K to 1400 K. As the wall temperature increases, increasing amounts of radiant energy are emitted from the wall. Hence, the net radiative heat flux on the wall decreases. Similarly, the convective heat flux decreases as the wall temperature increases, as the temperature gradient near the wall is decreased.

Finally, the effect of the wall emissivity on the wall heat flux is depicted in Fig. 9. The overall mixture ratio of oxygen to kerosene and the wall temperature are taken to be 2.34 and 1100 K, respectively. Because the leaving intensity from the wall is a summation of emitted and reflected intensities, the radiative heat flux increases as the emissivity increases. When the emissivity varies from 0.2 to 1.0, the radiative heat flux increases by about 4 times, while the conductive flux remains nearly constant. This is because there are very small changes in flow temperature and temperature gradient near the wall.

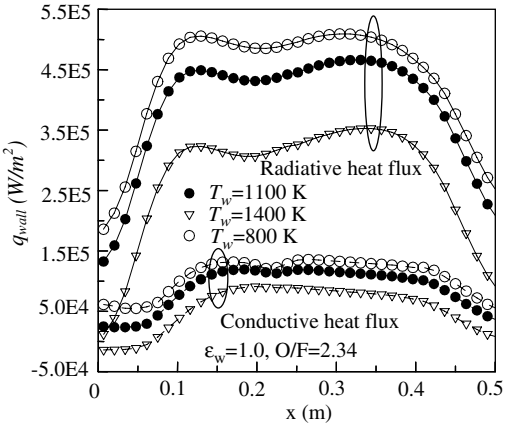

Fig. 8. Comparison of conductive and radiative heat fluxes on the wall for wall temperatures.

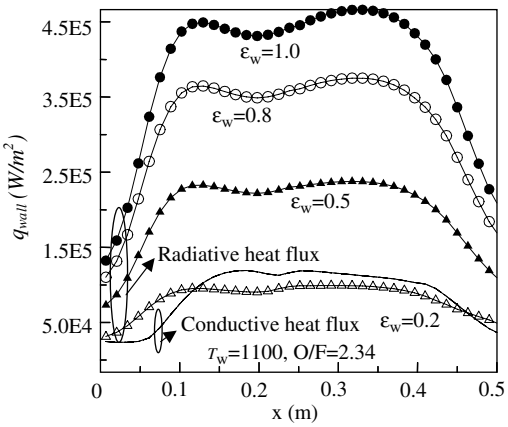

Fig. 9. Comparison of conductive and radiative heat fluxes on the wall for wall emissivities.

5. Conclusions

The present pressure-based method successfully predicts the liquid kerosene-oxygen spray combustion in the liquid fuel rocket engine at all speeds. In this study, soot formation at high temperatures and in a high pressure combustor is also investigated using a two-step global model. In particular, the effect of radiation on the thermo-fluid behavior is considered. The finite-volume method (FVM) is employed to solve the radiative transfer equation. Non-gray radiation by CO_2 and H_2O are modeled by the weighted-sum-of-gray-gases model (WSGGM), and the gray soot particulates are mixed with the non-gray gas. For the spray combustion flow in a liquid fuel rocket engine, the high temperature zone becomes smaller due to the radiant energy loss. The results of this study show that the effect of radiation on the heat transfer to the wall may be significant. As the effect of the soot particulates is dominant on the radiation, especially in a high pressure and high temperature combustor, accurate modeling of the soot formation becomes necessary.

Acknowledgement

This work was supported by the faculty research fund of Konkuk University in 2004.

References

[1] K.H. Chen, J.S. Huen, A coupled multi-block solution procedure for spray combustion in complex geometries, AIAA Paper 93-0108, 1993.
[2] C. Gueret, M. Cathonnet, J.C. Boettner, F. Gillard, Experimental Study and Modeling of Kerosene Oxidation in a Jet Stirred Flow Reactor, 23rd Symposium (International) on Combustion, The Combustion Institute, 1990, pp. 211–216.
[3] T.L. Jiang, H.H. Chiu, Bipropellant combustion in a liquid rocket combustion chamber, J. Propulsion Power 8 (5) (1992) 995–1003.
[4] C.E. Choi, S.W. Baek, Numerical analysis of a spray combustion with non-gray radiation using weighted sum of gray gases model, Combust. Sci. Technol. 115 (1996) 297–315.
[5] C.T. Crowe, M.P. Sharma, D.E. Stock, The particle source in cell (PSI-Cell) model for gas droplet flows, J. Fluid Eng. 99 (1997) 325–332.
[6] J.H. Ferziger, M. Peric, Computational Methods for Fluid Dynamics, Springer, 1996.
[7] I. Demirdzic, Z. Lilek, M. Peric, A collocated finite-volume method for predicting flows at all speeds, Int. J. Numer. Methods Fluids 16 (1993) 1029–1050.
[8] K.C. Karki, S.V. Patankar, Pressure-based calculation procedure for viscous flows at all speeds in arbitrary configuration, AIAA J. 27 (9) (1989) 1167–1174.
[9] J. Liu, S.N. Tiwari, Radiative heat transfer effects in chemically reacting nozzle flows, J. Thermophys. Heat Transfer 10 (3) (1996) 436–444.
[10] H.F. Nelson, Radiative heating in scramjet combustor, J. Thermophys. Heat Transfer 11 (1) (1997) 59–64.
[11] T. Badinand, T.H. Fransson, Radiative heat transfer in film-cooled liquid rocket engine nozzles, J. Thermophys. Heat Transfer 17 (1) (2003) 29–34.
[12] L. Tesse, F. Dupoirieux, J. Taine, Monte Carlo modeling of radiative transfer in a turbulent sooty flame, Int. J. Heat Mass Transfer 47 (2004) 555–572.
[13] T.E. Daubert, R.P. Danner, Physical and Thermodynamic Properties of Pure Chemicals, Hemisphere Pub. Co., New York, 1989.
[14] R.C. Reid, T.K. Sherwood, J.M. Pransnitz, The Properties of Gases and Liquids, McGraw-Hill, New York, 1987.
[15] G.M. Faeth, Evaporation and combustion of spray, Progr. Energy Combust. Sci. 9 (1983) 1–76.
[16] H.K. Versteeg, W. Malalasekera, An Introduction to Computational Fluid Dynamics – The finite-volume Method, Longman Scientific and Technical, 1995.
[17] C.D. Stewart, K.J. Syed, J.B. Moss, Modeling soot formation in non-premixed kerosene flames, Combust. Sci. Technol. 75 (1991) 211.
[18] G.M. Makhaviladze, J.P. Roberts, S.E. Yakush, Combustion of two-phase hydrocarbon fuel clouds released into the atmosphere, Combust. Flame 118 (1999) 583–605.
[19] M.J. Yu, S.W. Baek, J.H. Park, An extension of the weighted sum of gray gases non-gray gas radiation model to a two-phase mixture of non-gray gas with particles, Int. J. Heat Mass Transfer 43 (2000) 1699–1713.
[20] R.D. Skocypec, D.V. Walters, R.D. Buckius, Spectral emission measurements from planar mixtures of gas and particulates, ASME J. Heat Transfer 109 (1987) 151–158.
[21] M.F. Modest, Radiative Heat Transfer, Mc-Graw Hill Inc., 1993.
[22] B.R. Adams, P.J. Smith, Modeling effects of soot and turbulence-radiation coupling on radiative transfer in turbulent gaseous combustion, Combust. Sci. Technol. 109 (1995) 121–140.
[23] S.W. Baek, M.Y. Kim, J.S. Kim, Non-orthogonal finite-volume solutions of radiative heat transfer in a three-dimensional enclosure, Numer. Heat Transfer B 34 (4) (1998) 419–437.
[24] D.Y. Byun, S.W. Baek, M.Y. Kim, Thermal radiation in discretely heated irregular geometry using Monte-Carlo finite-volume and modified discrete-ordinate interpolation method, Numer. Heat Transfer A 37 (1999) 1–18.
[25] S.J. Kang, A Study of Droplet Size and Flow Characteristics of Injector, Korea Aerospace Research Institute Report, 1999.
[26] K.J. Young, C.D. Stewart, J.B. Moss, Soot formation in turbulent non-premixed kerosene-air flames burning at elevated pressure: experimental measurement, Proc. Combust. Instit. 25 (1994) 609.
[27] B.A. Fischer, J.B. Moss, The influence of pressure on soot production and radiation in turbulent kerosene spray flames, Combust. Sci. Technol. 138 (1998) 43.